Inorganic Chemistry

Article

pubs.acs.org/IC

Substitutional Mechanism of Ni into the Wide-Band-Gap Semiconductor $InTaO_4$ and Its Implications for Water Splitting Activity in the Wolframite Structure Type

Andrew C. Malingowski,[†] Peter W. Stephens,[‡] Ashfia Huq,[⊥] Qingzhen Huang,[#] Syed Khalid,[∥] and Peter G. Khalifah*[,†,§]

[†]Department of Chemistry and [‡]Department of Physics, State University of New York—Stony Brook, Stony Brook, New York 11794-3400, United States

[§]Department of Chemistry and [∥]National Synchrotron Light Source, Brookhaven National Laboratory, Upton, New York 11973-5000, United States

[⊥]Oak Ridge National Laboratory, Oak Ridge, Tennessee 37831-6475, United States

[#]NIST Center for Neutron Research, National Institute of Standards and Technology, Gaithersburg, Maryland 20878-9957, United States

Supporting Information

ABSTRACT: The mechanism of Ni substitution into the oxide semiconductor $InTaO_4$ has been studied through a combination of structural and spectroscopic techniques, providing insights into its previously reported photoactivity. Magnetic susceptibility and X-ray absorption near-edge spectroscopy (XANES) measurements demonstrate that nickel is divalent within the host lattice. The combined refinement of synchrotron X-ray and neutron powder diffraction data indicates that the product of Ni doping has the stoichiometry of $(In_{1-x}Ni_{2x/3}Ta_{x/3})TaO_4$ with a solubility limit of $x \approx 0.18$, corresponding to 12% Ni on the In site. Single-phase samples were only obtained at synthesis temperatures of 1150 °C or higher due to the sluggish reaction mechanism that is hypothesized to result from small free energy differences between $(In_{1-x}Ni_{2x/3}Ta_{x/3})TaO_4$ compounds with different x values. Undoped $InTaO_4$ is shown to have an indirect band gap of 3.96 eV, with direct optical transitions becoming allowed at photon energies in excess of 5.1 eV. Very small band-gap reductions (less than 0.2 eV) result from Ni doping, and the origin of the yellow color of $(In_{1-x}Ni_{2x/3}Ta_{x/3})TaO_4$ compounds instead results from a weak $^3A_{2g} \rightarrow {}^3T_{1g}$ internal $d \rightarrow d$ transition not associated with the conduction or valence band that is common to oxide compounds with Ni^{2+} in an octahedral environment.

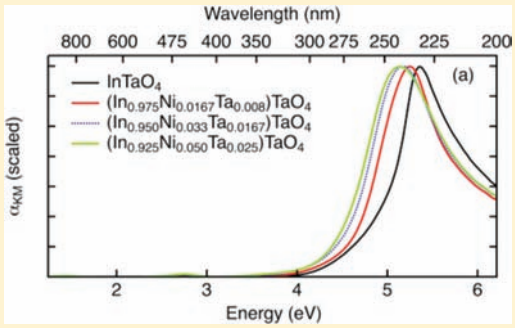

INTRODUCTION

Solar energy has the potential to supply global energy needs in a clean and renewable manner but currently only accounts for a very small fraction of global energy production due to the relatively high cost of its implementation. While most efforts to obtain electricity from the sun focus on production of electricity using photovoltaic (PV) devices, energy produced in this manner has high variations in its daily and seasonal output, cannot be easily stored, and requires a direct connection to existing electrical grids to be useful on the large scale. An alternative method for harvesting solar energy is to use a light-absorbing semiconductor to convert solar photons into a chemical fuel through the process of photoelectrolysis, where water is split to produce H_2 fuel through the reaction $2H_2O \rightarrow 2H_2 + O_2$. The reaction product of H_2 is a versatile energy currency which can be either converted into electricity with high efficiency (~60%) using a fuel cell,[1] burned like gasoline and natural gas, or converted into traditional petroleum-derived hydrocarbons using Fischer–Tropsch reactions, allowing compatibility with current energy technologies via the chemical reaction $(2n + 1)H_2 + nCO \rightarrow C_nH_{2n+2} + nH_2O$.[2]

While the process of semiconductor water splitting is well known,[3] the best stable semiconductors for driving it discovered to date convert solar radiation to chemical fuel with an overall efficiency of less than 1%. Substantial improvements in efficiency are needed before this process can become a viable technology. One of the biggest barriers limiting photoelectrolysis efficiency is the scarcity of visible-light-absorbing semiconductors (band gaps < 3.0 eV) that can drive this water splitting process. Although thermodynamic arguments suggest that photons with energies as small as 1.5 eV could potentially drive this process (1.23 V potential difference for

Received: December 21, 2011
Published: April 24, 2012

   dx.doi.org/10.1021/ic202715c | Inorg. Chem. 2012, 51, 6096–6103

the half reactions of H_2 production and O_2 production plus a small overpotential), no materials capable of direct solar water splitting (in the absence of an external bias) with band gaps less than 3.0 eV were discovered in the first 30 years of research in this field.

There was therefore great excitement following the 2001 *Nature* report by Zou et al.[4] that reported for the first time direct water splitting by a medium band-gap semiconductor. The band gap of $InTaO_4$ was reported to be reduced from 2.6 to 2.3 eV when Ni was substituted for In, and aqueous suspensions of powders with formulas $In_{1-x}Ni_xTaO_4$ ($0 < x < 0.15$) were reported to be active in producing both H_2 and O_2 gas when illuminated by light with $\lambda > 420$ nm (2.95 eV) when functionalized with a NiO cocatalyst to aid with H_2 production. However, there were a number of unusual aspects of this report. The stoichiometry of $In_{1-x}Ni_xTaO_4$ assumes a Ni^{3+} oxidation state, which is unexpected for the reported synthesis conditions (1100 °C in air) and was never directly investigated. The maximum activity was found for the $x = 0.10$ sample and not the sample at the reported Ni solubility limit of $x = 0.15$. Finally, the experimentally determined 2.6 eV band gap of $InTaO_4$ is substantially smaller than that of other tantalates such as Ta_2O_5 (4.6 eV[5]) and $Ca_2Ta_2O_7$ (4.4 eV[6]), perhaps indicating design principles that can be used for designing novel water splitting semiconductors with visible light activity.

It should be noted that the experimentally determined 2.6 eV band gap of $InTaO_4$ was substantially smaller than the 3.5–3.7 eV gaps later obtained from DFT calculations[7] despite the fact that DFT methods are known to substantially underestimate the magnitude of semiconductor band gaps.[7b,c,8] On the basis of trial DFT calculations, this discrepancy was suggested[7b,c] to arise from oxygen vacancies within the material, an as-yet experimentally unverified hypothesis. It has also been suggested previously that the true gap of this compound is reflected in the strong absorption feature at 4.3 eV rather than in the much weaker lower energy features,[9] a result supported by recent reflection electron energy loss spectroscopy (REELS) studies on $InTaO_4$ films prepared by physical vapor deposition.[10] Given the extensive ongoing interest in this system, we initiated a comprehensive structural and electronic characterization of pristine and Ni-doped $InTaO_4$ with the goal of understanding and reconciling the unusual properties reported for this system.

$InTaO_4$ crystallizes in the wolframite structure type (Figure 1) with the monoclinic space group $P2/c$ (no. 13).[11] This structure typically forms with an ABO_4 stoichiometry, where the *B*-site cation is an early $4d/5d$ transition metal (Nb, Mo, Ta, or W) and the *A* site is typically a different-sized transition metal or *p*-block cation. It is comprised of hexagonally close-packed oxygens with cations filling one-half of the available octahedral holes. The octahedra formed around the *A* and *B* cations form separate infinite edge-sharing "zigzag" chains that run along the *c* direction. These chains share corners with chains of the other cation type, forming offset layers stacked in the *a* direction. The wolframite structure type is tolerant of ionic substitution, and examples of wolframite compounds exist with mixed occupancies on both of the cation sites as well as on the anion site (in fluorinated compounds).[12] The substantially different ionic radii[13] of In^{3+} (0.80 Å) and Ta^{5+} (0.64 Å) can be comfortably accommodated via the distinctly different local environments of the *A*- and *B*-site cation positions. However, if the *A*-site and *B*-site cation radii are too close in size, cation disorder occurs and a smaller orthorhombic cell occurs, as is observed for $GaTaO_4$.[11] For Ni-doped $InTaO_4$, the Ni is

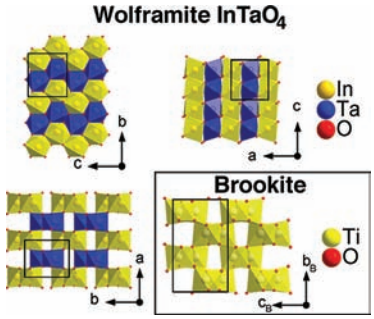

Figure 1. Three views of the structure of wolframite-type $InTaO_4$, which contains alternating edge-sharing chains of TaO_6 octahedra (blue) and InO_6 octahedra (gold) that run along the *c*-axis direction. (Inset) Structure of the brookite form of TiO_2. Structures of brookite TiO_2 (*Pnma*, $a = 5.16$ Å, $b = 9.25$ Å, $c = 5.46$ Å, inset) and wolframite $InTaO_4$ ($P2/c$, $a = 5.16$ Å, $b = 5.77$ Å, $c = 4.83$ Å, $\beta = 91.4°$) are very similar, and lattice parameters of the brookite (B) cell are related to the wolframite (W) cell via the relationships $a_B \approx c_W$; $b_B \approx 2a_W$; $c_B \approx b_W$.

believed to substitute only on the In site and known to cause a decrease in the length of the unit cell axes when substituted at concentrations up to its solubility limit (15–20% substitution),[14] an effect that is greatest along the *a* axis, which decreases at about twice the rate of the *b* and *c* axes.[14] There is substantial variation in the ionic radius of octahedral Ni depending on its valence state and whether it is in the high-spin (HS) or low-spin (LS) state, with tabulated ionic radii[13] of 0.48 (4+, LS), 0.56 (3+, LS), 0.60 (3+, HS), or 0.69 Å (2+). If the Ni cation is smaller than Ta, it might be expected to displace Ta from the *B* site to the *A*-cation site rather than directly substitute for In on the *A* site.

The wolframite compound $InTaO_4$ is chemically analogous to brookite, with equimolar amounts of In^{3+} and Ta^{5+} cations present in the place of the Ti^{4+} which is present in brookite-type TiO_2. The wolframite structure is also closely related to that of orthorhombic brookite, which has a similar arrangement of edge-sharing octahedral chains (Figure 1, with the relationship between their lattice parameters given in the figure caption). One subtle difference is that the close-packed oxygen layers in the wolframite structure are hexagonally close packed (AB), while those in the brookite structure have a mixed closed-packed arrangement (ABAC) involving both hexagonal and cubic motifs. This leads to roughly a doubled length of the brookite cell normal to the close-packed oxygen relative to the wolframite cell planes (brookite *b*-axis direction in space group *Pbca*, and the wolframite *a*-axis direction in space group $P2/c$).

The utility of $InTaO_4$ for visible-light-driven water splitting was initially remarked upon by Zou et al. in 2000,[15] where H_2 production was observed at a rate of about 2 μL/h (0.5 g sample, 300 W Xe lamp, 420 nm cutoff filter) using a NiO_x cocatalyst. In follow-up studies, Ni doping of $InTaO_4$ was found to improve H_2 production under the same conditions to values up to ~15 μL/h (quantum yield of ~0.7% at 402 nm), accompanied by approximately stoichiometric O_2 production.[4] Slightly lower activities were observed when a RuO_2 cocatalyst was used instead of NiO_x. Other 3d dopants than Ni were later found to reduce the visible light activity of this system relative to pure $InTaO_4$, though modest activities for H_2 production from a methanol sacrificial reagent (50–500 μL/h from a 1 g sample illuminated by a 400 W Hg lamp) were robustly found in both doped and undoped samples.[16] The water splitting

dx.doi.org/10.1021/ic202715c | Inorg. Chem. 2012, 51, 6096–6103

activity of this material was recently revisited by Douiheche et al., who observed mild activity for overall water splitting (up to ~6 μL/h H_2 production but with O_2 production substantially below stoichiometric levels for 0.3 g samples illuminated with a 150 W Hg lamp).[17] Curiously, activity was only observed in the absence of functionalization with a cocatalyst such as NiO_x, and Ni doping of $InTaO_4$ was not found to improve the UV response of this system.

EXPERIMENTAL SECTION

Three sample sets were prepared with the nominal compositions $In_{1-x}Ni_xTaO_4$ (x = 0.05, 0.10, 0.15, and 0.20), $(In_{1-x}Ni_{2x/3}Ta_{x/3})TaO_4$ (x = 0.025, 0.050, 0.075, 0.10, 0.15, 0.225, and 0.30), and $In_{0.9}Ni_xTaO_4$ (x = 0.05, 0.075, 0.10). Stoichiometric amounts of In_2O_3 (Alfa Aesar, 99.993%), Ta_2O_5 (Alfa Aesar, 99.994%), and NiO (Alfa Aesar, 99.998%) were ground together in an agate mortar and pestle under acetone. The reagents were placed in dense alumina crucibles and reacted at 1150 °C in air with regrinding every 24 h. Each reaction's progress was checked with X-ray powder diffraction on a Bruker D8 Advance laboratory diffractometer (λ = 1.54059 Å) using 12 mm variable slits and a 192-channel Lynx-Eye linear strip detector. When possible, samples were reacted until the X-ray diffraction patterns showed them to be free of In_2O_3 or Ta_2O_5 impurities within the detection limit of the diffractometer, estimated to be less than 1 wt % for this system.

The set of "Ni-deficient" samples with nominal composition $In_{0.9}Ni_xTaO_4$ (x = 0.05, 0.075, 0.10) was specifically prepared for X-ray absorption near-edge structure (XANES) analysis at the Ni K-edge, (8.333 keV), as the low Ni content ensured that the only Ni-containing phase would be Ni-doped $InTaO_4$ even though the exact stoichiometry of this phase was not yet known. Fluorescence data were collected using a Canberra PIPS (passivated implanted planar silicon) detector on beamline X19A (2.1−16.5 keV) at the National Synchrotron Light Source (NSLS) located at Brookhaven National Lab (BNL). X19A is equipped with a Si(111), double-crystal, fixed-exit height monochromator with feedback on the second crystal. The monochromator crystals were detuned to reject harmonics. The beam was collimated by a spherical mirror of Rh-coated glass and focused by a toroidal mirror of Rh-coated glass. Due to the relatively low Ni content and the high absorption coefficient of the host $InTaO_4$ matrix (8.3 μm X-ray absorption length), it was found that the best signal-to-noise could be obtained in fluorescence rather than transmission mode, and therefore, only fluorescence data are presented. Data were processed with the program ATHENA, part of the Horae software package.[18]

Standards used for determining the Ni-dopant edge energy were Ni-metal foil, NiO, and $KNiIO_6$, representing Ni oxidation states of 0, 2+, and 4+, respectively. The Ni foil was provided by beamline X-19A, and the NiO was purchased from Alfa Aesar (99.998% pure). $KNiIO_6$ was prepared using the procedure outlined by Murphy.[19] Powder samples and standards were ground with an agate mortar and pestle and spread over a piece of Scotch tape approximately 1 m long, which was then folded over multiple times and sealed on the edges with more tape. A Ni-metal foil reference was placed in the beam path after the sample and used to calibrate the energies of the absorption data.

Magnetic susceptibility data were collected using the Vibrating Sample Magnetometer option on a Physical Properties Measurement System (PPMS) manufactured by Quantum Design. Powder samples were measured in clear plastic sample holders supplied by Quantum Design for use with the instrument and held in place with clear two-part epoxy. Measurement of an empty sample holder showed a small diamagnetic response that has no appreciable effect on data interpretation. Samples were measured using both zero-field-cooled and field-cooled scans in magnetic fields of 0.1, 1, and 5 T over a temperature range from 300 to 2 K. Data were fit to a modified Curie−Weiss law using the program Igor Pro.[20]

High-resolution X-ray powder diffraction data used in the X-ray neutron corefinements were taken at the National Synchrotron Light Source (NSLS) beamline X16C. Data was collected using a λ = 0.69755 Å over a range of 5−50° 2θ (0.8−8 Å^{-1} d spacing). X16C uses a parallel-beam setup employing a channel-cut Si(111) monochromator and a Ge(111) analyzer crystal giving $\Delta d/d \approx 2 \times 10^{-4}$. The exposure time was increased as the scan progressed to increase counting statistics at low d spacing.

Constant wavelength neutron diffraction data were collected on preliminary $In_{1-x}Ni_xTaO_4$ samples at the BT-1 high-resolution powder diffractometer located at the National Institute of Standards and Technology. Measurements were taken with a neutron wavelength of 1.54030 Å using a Cu(311) monochromator over a range of 2.5−167° 2θ.

Time-of-flight (TOF) neutron diffraction data were collected on the POWGEN instrument in the Spallation Neutron Source (SNS) located at Oak Ridge National Laboratory (ORNL). Data was collected at a temperature of 300 K using a proton pulse rate of 30 Hz, 1.5×10^{14} protons/pulse. Collection times varied from approximately 8.3 to 5.5 h. Three detector banks were used at 155°, 85°, and 45° with ranges of 12−34 μm, 11−33 μs, and 8−50 μs respectively. The resolution in terms of $\Delta d/d$ is between 0.01 and 0.02 over the measured range in d space of 0.45−4.05 Å.

Diffuse reflectance data were collected on a Perkin-Elmer Lambda 950 Spectrophotometer over a range of 200−1000 nm (1.24−6.20 eV). $BaSO_4$ was used as a 100% reflectance standard. Sample responses in the far-UV range were also checked using larger band-gap Al_2O_3 standard and found to be consistent with the $BaSO_4$ data.

RESULTS AND DISCUSSION

In the initial synthesis trials, samples with the nominal stoichiometry $In_{1-x}Ni_xTaO_4$ were heated for 48 h at 1100 °C, a temperature routinely used to prepare these materials. This synthesis method always produced samples that clearly contained In_2O_3 as well as NiO impurities. In addition to these impurities, high-resolution powder diffraction experiments performed on NSLS beamline X16C (Figure 2) showed that

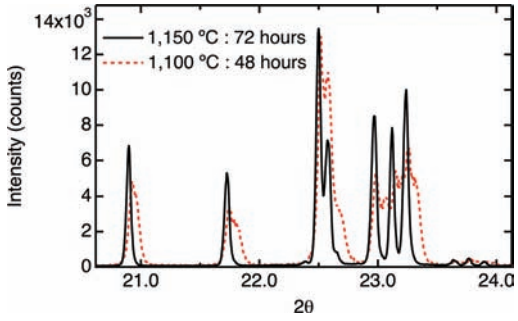

Figure 2. Samples of "$In_{0.9}Ni_{0.1}TaO_4$" heated for 48 h at 1100 °C (red, dashed) and 72 h at 1150 °C (solid, black). Peaks of the sample synthesized at 1100 °C are split indicating the presence of two wolframite phases of slightly different composition, a problem that is resolved by heating samples hotter and longer.

the wolframite X-ray peaks are split, indicating the presence of two separate wolframite phases with different compositions. The kinetic reasons for this will be discussed later. Increasing the temperature to 1150 °C and increasing the heating time to 72 h produced samples that did not show this peak splitting or In_2O_3 impurities; however, the NiO impurity persisted. All subsequent samples were reacted at 1150 °C until the X-ray diffraction data indicated the reaction was complete (no noticeable split peaks, a stable unit cell size, no change in phase fractions).

Both synchrotron and lab X-ray diffraction patterns of $In_{1-x}Ni_xTaO_4$ samples show a small but noticeable impurity that can be assigned to the NiO 200 diffraction peak, which persisted

dx.doi.org/10.1021/ic202715c | Inorg. Chem. 2012, 51, 6096−6103

even after the wolframite phase appeared to reach equilibrium (Figure 3). This NiO impurity phase was much more apparent

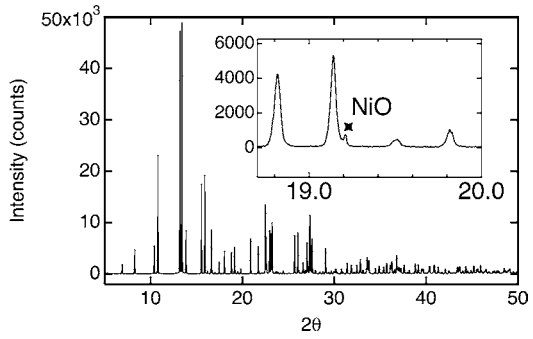

Figure 3. Synchrotron X-ray diffraction pattern, collected at NSLS beamline X16C, which results from heating a sample with a nominal stoichiometry of "$In_{0.90}Ni_{0.10}TaO_4$". (Inset) Most visible peak of the NiO impurity phase.

in the neutron powder diffraction data collected on these samples due to the high neutron cross-section of Ni relative to the other elements present. The presence of NiO in equilibrated samples shows that the true stoichiometry of Ni-doped $InTaO_4$ is Ni deficient relative to $In_{1-x}Ni_xTaO_4$, suggesting that the Ni valence is unlikely to be 3+.

Our first step in determining the correct stoichiometery of Ni-doped $InTaO_4$ was to use X-ray absorption near-edge spectroscopy (XANES) at the Ni K-edge to make a direct measurement of the Ni oxidation state. Although single-phase samples were not available, the element-specific nature of the technique ensures that impurity phases without Ni will not affect the measured X-ray absorption spectrum. For this reason, the stoichiometries of several samples were purposely made Ni deficient (compositions of $In_{0.9}Ni_xTaO_4$ with x = 0.10, 0.075, 0.05) and reacted until powder X-ray diffraction experiments showed that there were no Ni-containing impurity phases that could affect the measured absorption edge energy. Determination of the oxidation state from XANES data was done by comparing the Ni X-ray absorption edge energy of Ni-doped $InTaO_4$ to a series of Ni-containing standards with known oxidation states (Figure 4). In all samples, the Ni absorption

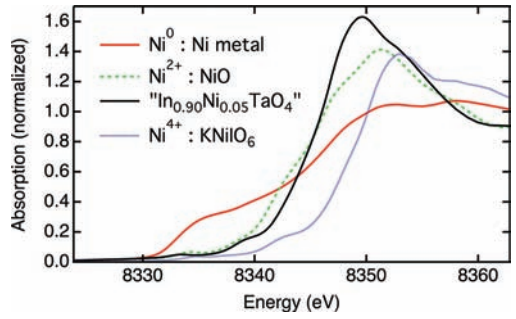

Figure 4. XANES data for a sample with the nominal composition $In_{0.90}Ni_{0.05}TaO_4$ reacted at 1150 °C. Sample Ni K-edge energy aligns with that of the NiO standard, demonstrating the presence of Ni^{2+} in Ni-doped $InTaO_4$.

edge best aligns with the 2+ standard, NiO, indicating that Ni-doped $InTaO_4$ contains Ni^{2+}.

Additional insights into the Ni valence and the distribution of Ni cations within the wolframite structure were obtained from magnetic susceptibility (χ_n) measurements on samples with compositions $(In_{1-x}Ni_{2x/3}Ta_{x/3})TaO_4$ with x = 0, 0.025, and 0.05 (Figure 5). Magnetic parameters determined from fits to a modified Curie–Weiss law of $\chi_n = \chi_0 + C/(T - \theta)$ are given in Table 2, where χ_n is the magnetic susceptibility, χ_0 is a temperature-independent diamagnetic contribution, C is the Curie constant, T is temperature, and θ is the Weiss constant. Single-phase $InTaO_4$ is essentially nonmagnetic, therefore, confirming that Ni is the only contributor to the paramagnetic susceptibility of Ni-doped $InTaO_4$. The Ni effective magnetic moment (μ_{eff}) is very effective in uniquely discriminating between the different oxidation states and spin states of octahedral Ni cations, as can be seen in Table 1. The effective

Table 1. Possible Spin States of Ni in $InTaO_4$, Associated Spin Number (S), and Corresponding Values for μ_{eff} Calculated from the Spin State

state	S	$(4S(S+1))^{1/2}$
Ni^{2+} d^8	0	0
Ni^{3+} d^7 low spin	1/2	1.73
Ni^{3+} d^7 high spin	3/2	2.83
Ni^{4+} d^6 low spin	0	3.87
Ni^{4+} d^6 high spin	2	4.90

moments fit to $(In_{1-x}Ni_{2x/3}Ta_{1/3x})TaO_4$ samples are most consistent with a Ni^{2+} (μ_{eff} = 2.83 μ_B) oxidation state. There are a few possible explanations for the observed excess moment. The very small mole fraction of Ni in these samples makes a precise moment determination challenging. Also, it is not uncommon to have a Ni^{2+} moment that exceeds the spin-only moment due to incomplete orbital quenching, and a range of 2.9–3.4 has been previously found to be common among Ni^{2+} species.[21] Finally, Ni is about 0.1 Å smaller than In^{3+} and is not necessarily expected to be found in ideal octahedral coordination, as will be discussed more later.

Following the results above, it is important to ask the following question: What is the substitutional mechanism of Ni^{2+} for In^{3+} in the wolframite $InTaO_4$ structure? There are two likely routes that could accommodate Ni^{2+} for In^{3+} substitution in the wolframite structure while maintaining overall charge balance. The first possibility is that Ni^{2+} stoichiometrically replaces In^{3+} and that charge balance is maintained through the loss of oxygen, giving an oxygen-deficient formula of $In_{1-x}Ni_xTaO_{4-x/2}$. We can rule out this model due to the consistent observation of an NiO impurity phase present in the X-ray patterns of samples synthesized with this cation stoichiometry. The second route for maintaining charge balance is the cosubstitution of Ni^{2+} and Ta^{5+} for In^{3+}, resulting in a stoichiometry of $(In_{1-x}Ni_{2x/3}Ta_{x/3})TaO_4$ and structures that are fully stoichiometric in oxygen. The relationship of these two substitutional models within the context of our proposed In_2O_3–Ta_2O_5–NiO equilibrium phase diagram at 1150 °C (based on the analysis of X-ray patterns for the four sets of stoichiometries synthesized during this work) is illustrated in Figure 6.

It can be clearly seen that all samples made with the originally proposed composition[4] of $In_{1-x}Ni_xTaO_4$ fall in the NiO–wolframite solid solution two-phase region and will therefore have NiO as the one and only impurity phase. This NiO impurity is quite easy to miss in conventional X-ray diffraction experiments due to the near-perfect peak overlap with the $InTaO_4$ wolframite peaks with the exception of one

dx.doi.org/10.1021/ic202715c | Inorg. Chem. 2012, 51, 6096–6103

Table 2. Experimentally Determined Modified Curie–Weiss Fit Constants and Resulting Effective Moments Fit from Zero-Field-Cooled Scans

50000 Oe ZFC	θ (K)	C (emu·K·mol^{-1})	μ_{eff} (μ_B)	χ_0 (emu·mol^{-1})
$InTaO_4$	−9.2(3)	0.000586(6)	0.068(4)	−0.00004026(8)
$(In_{0.975}Ni_{0.0167}Ta_{0.008})TaO_4$	−3.16(2)	1.278(1)	3.20(7)	−0.00297(1)
$(In_{0.950}Ni_{0.033}Ta_{0.0167})TaO_4$	−3.79(8)	1.289(5)	3.21(1)	−0.001311(4)

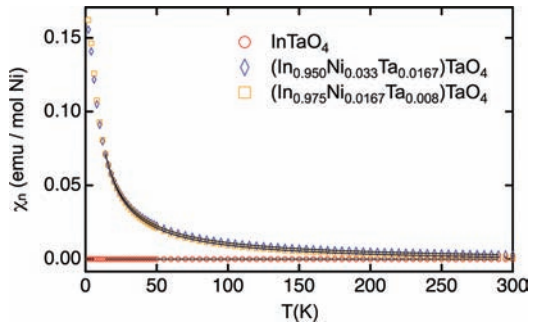

Figure 5. Temperature-dependent magnetic susceptibility of $(In_{1-x}Ni_{2x/3}Ta_{x/3})TaO_4$ samples with x = 0, 0.025, and 0.05. Curie–Weiss fits to the data are shown in black.

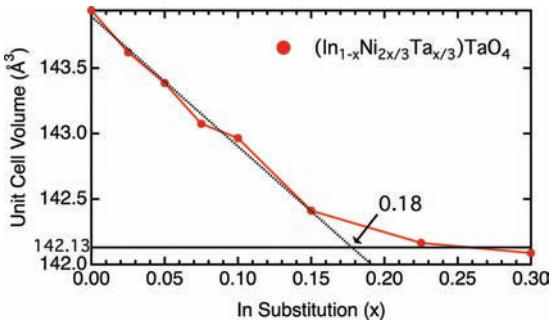

Figure 7. Cell volume of $(In_{1-x}Ni_{2x/3}Ta_{x/3})TaO_4$ decreases with increasing Ni content, reaching a minimum volume at about 142.1 Å^3 (dotted line).

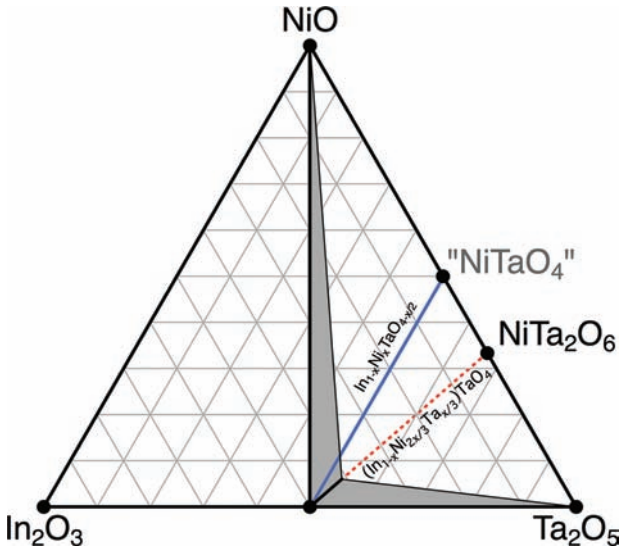

Figure 6. Phase diagram of In_2O_3, Ta_2O_5, and NiO at 1150 °C in air. Dashed red line marks the $(In_{1-x}Ni_{2x/3}Ta_{x/3})TaO_4$ stoichiometry, and actual solid solution region is highlighted in black. Samples made with the initial composition $In_{1-x}Ni_xTaO_4$ fall on the blue line crossing the NiO–wolframite two-phase region. Only the right half of the phase diagram was directly investigated in this work.

peak at $d \approx 2.09$ Å that may show up as a peak shoulder. Single-phase samples can be made with the $(In_{1-x}Ni_{2x/3}Ta_{x/3})TaO_4$ stoichiometry until the solubility limit of Ni is reached; higher x values will result in a two-phase mixture of $NiTa_2O_6$ with maximally doped wolframite, a result we confirmed experimentally using a series of samples with compositions of $(In_{1-x}Ni_{2x/3}Ta_{x/3})TaO_4$ with x = 0.025, 0.050, 0.075, 0.10, 0.15, 0.225, and 0.30. The solubility limit was quantified both by following the lattice parameter variation of these samples (Figure 7) obtained through a fundamental parameters Rietveld refinement and by the lever-rule analysis of wolframite/$NiTa_2O_6$ phase fractions of samples beyond the solubility limit. The maximum level of Ni doping at 1150 °C was found to be 12%, corresponding to a value of x = 0.18.

It should be noted that extremely long reaction times (greater than 380 h) at 1150 °C were needed to equilibrate to single-phase samples and that incompletely reacted samples had noticeably larger cell volumes than the final products. This might explain the variability in the lattice parameters reported by different groups[14,17] and suggests that even higher Ni substitution levels could potentially be obtained at higher reaction temperatures. The sluggish kinetics for the equilibration of the solid solution may be related to the phase behavior of this system. $NiTa_2O_6$ rapidly forms along with a Ni-deficient (relative to the starting stoichiometry) wolframite phase as the starting material is consumed. Continued heating causes the $NiTa_2O_6$ impurity phase to diminish, with the shifting mass balance causing the wolframite phase unit cell to shrink as more Ni is incorporated into this phase in a process that is slow due to the relatively low free energy differences involved between wolframite phases with different Ni concentrations.

Neutron powder diffraction experiments offer the possibility of accurately probing oxygen contents, and tests of the putative $In_{1-x}Ni_xTaO_{4-x/2}$ structural model as well as free refinements of the oxygen occupancies provided no evidence for oxygen vacancies. Combined refinements of the neutron diffraction data and synchrotron X-ray data were carried out to have good sensitivity to species on triply occupied sites suggested by our proposed $(In_{1-x}Ni_{2x/3}Ta_{x/3})TaO_4$ stoichiometry. The large differences in the atomic scattering factors between X-rays and neutrons give two different and complementary pictures of the system that result in a more stable refinement than is possible from analyzing the data sets separately. However, due to the complexity of refining a triply occupied site, refinement of the $(In_{1-x}Ni_{2x/3}Ta_{x/3})TaO_4$ structure still required a variety of restraints to guarantee a valid crystal structure.

First, the stoichiometry of the model was constrained so that charge balance is maintained. Second, the atomic displacement parameters (ADPs) of all the atoms residing on the indium site were constrained to be equal, although this is likely not the case due to the large differences in Ni, In, and Ta radii and masses. The phase fractions and scale factors of the different data sets collected on identical samples were constrained so that the fraction of any phases present were constant among them.

dx.doi.org/10.1021/ic202715c | Inorg. Chem. 2012, 51, 6096–6103

Lastly, the X-ray data sets were down-weighted by a factor of 3 to prevent them from dominating the refinements due to their much higher counting statistics relative to the neutron data. Within these constraints, no evidence for oxygen deficiency was found. The final structural model was able to very effectively simultaneously model the X-ray and neutron data sets. The experimentally determined phase fractions and final structural parameters determined from this analysis are tabulated in Table 3.

Table 3. Final Cell Parameters and Phase Fractions for $(In_{1-x}Ni_{2x/3}Ta_{x/3})TaO_4$ Determined from X-ray/Neutron Rietveld Corefinements

formula	$InTaO_4$	$(In_{0.95}Ni_{0.033}Ta_{0.017})TaO_4$	$(In_{0.90}Ni_{0.066}Ta_{0.033})TaO_4$
a (Å)	4.830251(2)	4.824528(3)	4.818630(2)
b (Å)	5.775132(2)	5.773787(3)	5.770230(3)
c (Å)	5.157150(1)	5.155303(3)	5.152369(2)
β (deg)	91.42510(3)	91.37640(3)	91.3467(4)
volume (Å^3)	143.8160(1)	143.5640(2)	143.2200(1)
R_p	0.0438	0.0539	0.0556
wR_p	0.0496	0.0532	0.0521
χ^2	0.9172	0.8348	0.9826
NiO impurity (wt %)		0.3(2)	0.9(1)

Given the revised composition of the Ni-doped wolframite phase, it was important to revisit the optical properties of this compound as secondary phases can interfere with the measurements of the intrinsic optical response. Diffuse reflectance measurements of $(In_{1-x}Ni_{2x/3}Ta_{x/3})TaO_4$ samples with x = 0, 0.025, 0.050, and 0.075 were collected to determine the magnitude and nature of the band gap. The raw reflectance (R) data were converted to units of relative absorption (α) via a Kubelka–Munk (KM) transform:[22] $\alpha(E) = (1 - R)^2/(2R)$.

For all compositions studied, the absorption spectra have their major feature associated with transitions across the band gap below 300 nm, far from the visible range (Figure 8a). In the Ni-containing samples there is a much less intense second feature in the visible region, centered at approximately 450 nm (2.8 eV). The intensity of this feature scales as the Ni content increases, but its position and shape do not change (Figure 8b).

The magnitudes of the optical band gaps (E_g) were determined from an analysis of the major absorption feature (Figure 8a). The slow onset of absorption by wolframite $InTaO_4$ is characteristic of an indirect band-gap semiconductor,[23] a result that quantitative fits confirmed. E_g was determined by fitting the absorption data to the function describing the optical absorption of an indirect band-gap semicondcutor: $\alpha(E) = A^*(E - E_g)^2/E$, where E is the photon energy expressed in eV and A is a constant.[23a] The photon energy (E) was included in the denominator of this equation to account for the typical energy dependence of the refractive index (n), though this has a minor influence on the fit results. In the case of pure $InTaO_4$, the indirect band gap was found to be 3.96 eV and the functional form for indirect band-gap absorbance was followed over the energy range of 4.2–4.7 eV (Figure 9a and 9b).

At higher photon energies, the $InTaO_4$ absorbance increased more quickly in a manner consistent with a direct optical transition with a gap of about 5.1 eV and can be easily visually seen when the data are rescaled (Figure 9c) to emphasize the

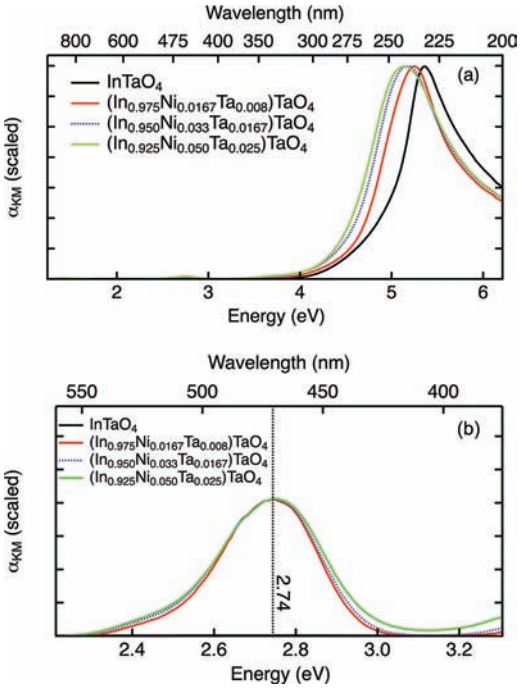

Figure 8. (a) Relative absorption calculated via a Kubelka–Munk transform for various x values of $(In_{1-x}Ni_{2x/3}Ta_{x/3})TaO_4$. Data shows a small shift in the band edge toward lower energies as the Ni content increases. (b) Weak absorption feature in the Ni-doped $InTaO_4$ absorption spectrum centered at 2.74 eV (453 nm) is the result of internal d → d transitions from the octahedrally coordinated Ni^{2+}.

scaling of a direct band-gap transition: $\alpha(E) = A^*(E - E_g)^{1/2}/E$.[23a] At lower photon energies, including energies below the band gap, the optical response was dominated by an Urbach tail that reflects a broadened distribution of electronic states around the gap energy.[23a] The function describing the Urbach tail is $\alpha_{Urbach}(E) = A^* \exp((E - E_g)k_BT/\sigma)$, where σ is an empirical parameter corresponding to the breadth of the distribution and k_B is the Boltzmann constant. The range where the Urbach response dominates (3.7–4.1 eV) can readily be seen from a plot of the logarithm of absorbance as a function of energy (Figure 9d).

When the same type of analysis is carried out on Ni-doped samples with compositions of $(In_{1-x}Ni_{2x/3}Ta_{x/3})TaO_4$ with x = 0.025, 0.050, and 0.075, the small influence of Ni on the size of the band gap can be seen (Table 4). With increasing Ni doping, the magnitude of the band gap (E_g) slightly decreases from the 3.96 eV of the pristine material by a few tenths of an electronvolt, but it clearly never moves into the visible light energy range. The optical changes are believed to result more from compression of the unit cell volume and broadening of the valence and conduction band rather than from electronic interactions between Ni and In/Ta states. The magnitude of the Urbach broadening (Table 4) was substantially larger in the doped samples than in pristine $InTaO_4$ and was generally independent of the amount of Ni.

However, Ni doping does induce a weak absorption peak in the visible regime (2.74 eV, 453 nm) that is not associated with excitations across the band gap. The position of this excitation is essentially independent of doping level, as can be seen when data at doping levels are scaled to match in intensity (Figure 8b). In a broad study of compounds containing octahedrally coordinated Ni^{2+}, it has previously been observed that there is an

dx.doi.org/10.1021/ic202715c | Inorg. Chem. 2012, 51, 6096–6103

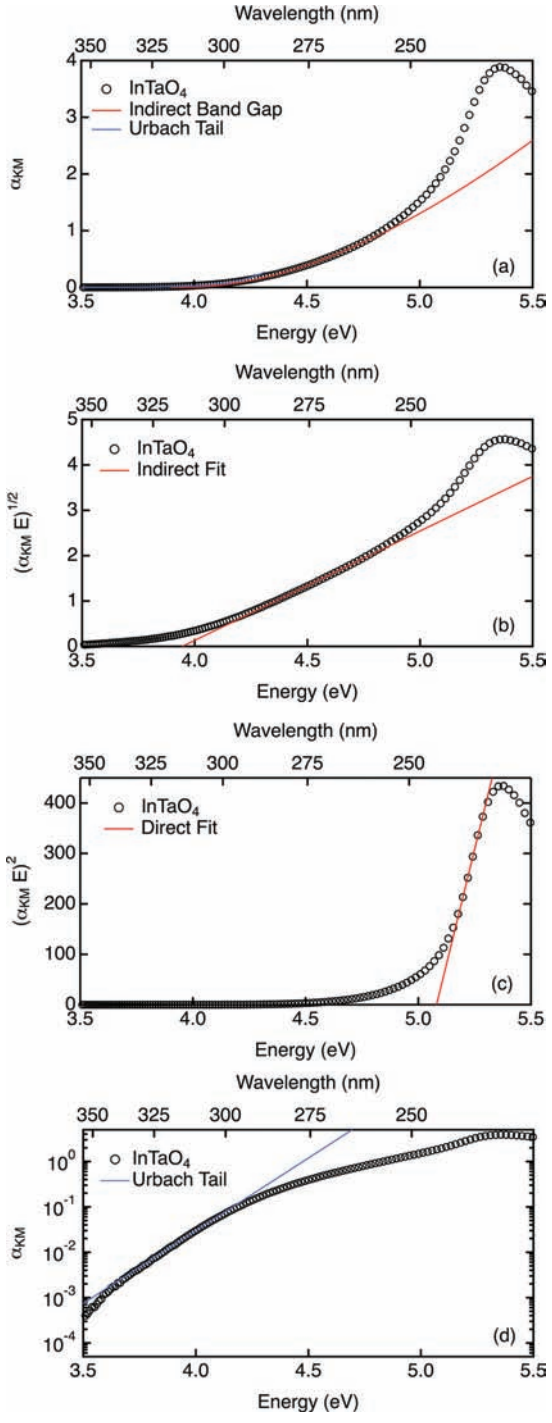

Figure 9. (a) Relative absorbance (α_{KM}) of $InTaO_4$ obtained from the Kubleka–Munk transform of diffuse reflectance data with overlaid fits of the fit of the indirect band gap (red) and Urbach tail (blue). Rescaled data is shown to emphasize the regions where the absorbance follows the functional form of (b) an indirect band-gap transition (4.2–4.7 eV), (c) a direct band-gap transition (5.2–5.4 eV), and (d) an Urbach tail (3.7–4.1 eV).

absorption feature at 400 nm range that is the result of a $^3A_{2g} \rightarrow {}^3T_{1g}$ (G) internal d → d transition.[24] The weak absorption feature seen in the Ni-doped $InTaO_4$ diffuse reflectance data is almost certainly the result of this local Ni excitation. Prior studies have also observed other internal Ni transitions at energies of approximately 800 and 1100 nm, excitations that were not clearly resolved in our data, probably due to the low concentration of Ni. These types of spin-forbidden internal transitions seem poorly suited for driving photochemical reactions such as overall water splitting.

Table 4. Indirect Band Gaps of $(In_{1-x}Ni_{2x/3}Ta_{x/3})TaO_4$ Samples

formula	band gap (eV)	σ_{urbach}
$InTaO_4$	3.958(3)	0.141(1)
$(In_{0.975}Ni_{0.017}Ta_{0.008})TaO_4$	3.819(9)	0.237(2)
$(In_{0.950}Ni_{0.033}Ta_{0.017})TaO_4$	3.809(8)	0.310(5)
$(In_{0.925}Ni_{0.050}Ta_{0.025})TaO_4$	3.787(9)	0.308(4)

These studies clearly demonstrate that the previously reported visible light activity for Ni-doped $InTaO_4$ cannot be due to the intrinsic properties of this material, which has an indirect band gap of 3.7–3.9 eV depending on the Ni content. A more likely source of the previously observed activity is a secondary phase. We demonstrated that NiO is a ubiquitous impurity for samples made with an $In_{1-x}Ni_xTaO_4$ stoichiometry and that samples heated at temperatures that are too low or for times that are too short can contain both In_2O_3 and Ta_2O_5 impurities. In particular, In_2O_3 is known to have visible light absorbance (E_g = 2.619[23b]) and activity for water splitting reactions.[25] Furthermore, the optical response of In_2O_3 can obscure the local nature of the transition centered at 2.7 eV in Ni-containing samples and has likely lead to the prior incorrect assignment of this feature as being representative of the optical band gap of Ni-doped $InTaO_4$.[4,14,26]

CONCLUSIONS

The synthesis, structure, and properties of Ni-doped $InTaO_4$ have been reinvestigated. XANES and magnetic susceptibility studies show that these phases contain Ni^{2+}, which can substitute for In^{3+} only when charge compensation with Ta^{5+} occurs. The general stoichiometry of these phases is $(In_{1-x}Ni_{2x/3}Ta_{x/3})TaO_4$, with a maximum x value of 0.18, which corresponds to incorporation of 12% Ni on the In position. Pristine $InTaO_4$ is found to be an indirect band-gap semiconductor (3.96 eV), and Ni does not reduce the gap below 3.7 eV. Additional weak optical transitions associated with internal transitions for octahedral Ni^{2+} are observed at 2.74 eV, but these are not likely to be relevant to the photochemistry of this system.

ASSOCIATED CONTENT

Supporting Information

This material is available free of charge via the Internet at http://pubs.acs.org.

AUTHOR INFORMATION

Corresponding Author

*E-mail: kpete@bnl.gov.

Notes

The authors declare no competing financial interest.

ACKNOWLEDGMENTS

This work was in part carried out at BNL under Contract DE-AC02-98CH10886 with the U.S. Department of Energy. We also gratefully acknowledge the U.S. DOE for funding under the BES Hydrogen Fuel Initiative. A portion of this Research at Oak Ridge National Laboratory's Spallation Neutron Source

was sponsored by the Scientific User Facilities Division, Office of Basic Energy Sciences, U.S. Department of Energy. Use of the National Synchrotron Light Source, Brookhaven National Laboratory, was supported by the U.S. Department of Energy, Office of Science, Office of Basic Energy Sciences, under Contract No. DE-AC02-98CH10886. We thank Saul Lapidus for his experimental assistance in utilizing beamline X16C. Diffuse reflectance data was collected at Brookhaven National Laboratory's Center for Functional Nanomaterials, which is supported by the Department of Energy under grant DE-AC02-98CH10886. We acknowledge the support of the National Institute of Standards and Technology, U.S. Department of Commerce, in providing the neutron research facilities used in this work.

REFERENCES

(1) Vishnyakov, V. M. *Vacuum* **2006**, *80* (1053−1065), 1053−1065.
(2) Dry, M. E. *Catal. Today* **2002**, *71*, 227−241.
(3) Honda, K.; Fujishima, A. *Nature* **1972**, *238*, 37−38.
(4) Zou, Z.; Ye, J.; Sayama, K.; Arakawa, H. *Nature* **2001**, *414*, 625−627.
(5) Strehlow, W. H.; Cook, E. L. *J. Phys. Chem. Ref. Data* **1973**, *2*, 163.
(6) Ikeda, S.; Fubuki, M.; Takahara, Y. K.; Matsumura, M. *Appl. Catal., A* **2006**, *300* (2), 186−190.
(7) (a) Matsushima, S.; Nakamura, H.; Arai, M.; Kobayashi, K. *Chem. Lett.* **2003**, *32* (1), 64−65. (b) Chang, H.; Kong, K.; Choi, Y. S.; Choi, Y.; Baeg, J.-O.; Moon, S.-J. *C.R. Chim.* **2006**, *9*, 841−845. (c) Chang, H.; Kong, K.; Choi, Y. S.; In, E.; Choi, Y.; Baeg, J.-O.; Moon, S.-J. *Chem. Phys. Lett.* **2004**, *398*, 449−452. (d) Oshikiri, M.; Boero, M.; Ye, J.; Zou, Z.; Kido, G. *J. Chem. Phys.* **2002**, *117* (15), 7313−7318.
(8) Matsushima; Shigenori; Obata, K.; Nakamura, H.; Arai, M.; Kobayashi, K. *J. Phys. Chem. Solids* **2003**, *64*, 2417−2421.
(9) Li, G.-L.; Yin, Z. *Phys. Chem. Chem. Phys.* **2011**, *13* (7), 2824−2833.
(10) Rico, V. J.; Frutos, F.; Yubero, F.; Espinos, J. P.; Gonzáles-Elipe, A. R. *J. Vac. Sci. Technol., A* **2010**, *28* (1), 127−134.
(11) Harneit, O.; Muller-Buschbaum, H. *J. Alloys Compd.* **1993**, *194*, 101−103.
(12) Villars, P.; Cenzual, K. *Pearson's Crystal Data: Crystal Structure Database for Inorganic Compounds (on CD-ROM)*, Version 1.0, 1.0; ASM International: Materials Park, OH, 2007/ 8.
(13) Shannon, R. D. *Acta Crystallogr., Sect. A: Found. Crystallogr.* **1976**, *A32* (5), 751−767.
(14) Zou, Z.; Ye, J.; Sayama, K.; Arakawa, H. *J. Mater. Res.* **2002**, *17* (6), 1419−1424.
(15) Zou, Z.; Ye, J.; Arakawa, H. *Chem. Phys. Lett.* **2000**, *332* (3−4), 271−277.
(16) Zou, Z.; Ye, J.; Abe, R.; Sayama, K.; Arakawa, H. Studies in Surface Science and Catalysis 2002. *Proceedings of the Fourth Tokyo conference on Advance Catalytic Science and Technology*; Elsevier: Amsterdam, 2003; Vol. *145*, pp 165−168.
(17) Douiheche, M.; Haberkorn, R.; Beck, H. P. *Z. Naturforsch., B: Chem. Sci.* **2008**, *63b*, 1160−1168.
(18) (a) Newville, M. *J. Synchrotron Radiat.* **2001**, *8*, 322−324. (b) Ravel, B. *J. Synchrotron Radiat.* **2001**, *8*, 314−316. (c) Ravel, B.; Newville, M. *J. Synchrotron Radiat.* **2005**, *12*, 537−541.
(19) Murphy, C. P.; Sethuram, B.; Rao, T. N. *Z. Phys. Chem., Leipzig* **1986**, *267* (6), 1212−1218.
(20) *IGOR Pro*, 6.12; WaveMetrics: Lake Oswego, OR, 2009.
(21) Cotton, F. A.; Wilkinson, G. *Advanced Inorganic Chemistry*, 5th ed.; Wiley-Interscience: New York, 1988.
(22) Kubelka, P.; Munk, F. *Z. Tech. Phys.* **1931**, *12*, 593.
(23) (a) Pankove, J. I. *Optical Properties in Semiconductors*; Dover Publications: New York, 1971. (b) Weiher, R. L.; Ley, R. P. *J. Appl. Phys.* **1966**, *37* (1), 299−302.
(24) Rossman, G. R.; Shannon, R. D.; Waring, R. K. *J. Solid State Chem.* **1981**, *39*, 277−287.
(25) Kudo, A.; Miseki, Y. *Chem. Soc. Rev.* **2009**, *38*, 253−278.
(26) (a) Zou, Z.; Ye, J.; Arakawa, H. *Mater. Res. Bull.* **2001**, *36*, 1185−1193. (b) Zou, Z.; Ye, J.; Arakawa, H. *Catal. Lett.* **2001**, *75* (3−4), 209−213. (c) Zou, Z.; Ye, J.; Arakawa, H. *J. Phys. Chem. B* **2002**, *106* (51), 13098−13101. (d) Zou, Z.; Ye, J.; Arakawa, H. *Int. J. Hydrogen Energy* **2003**, *28*, 663−669. (e) Zou, Z.; Ye, J.; Sayama, K.; Arakawa, H. *J. Photochem. Photobiol., A* **2002**, *148*, 65−69. (f) Zou, Z.; Arakawa, H. *J. Photochem. Photobiol., A* **2003**, *158*, 145−162.